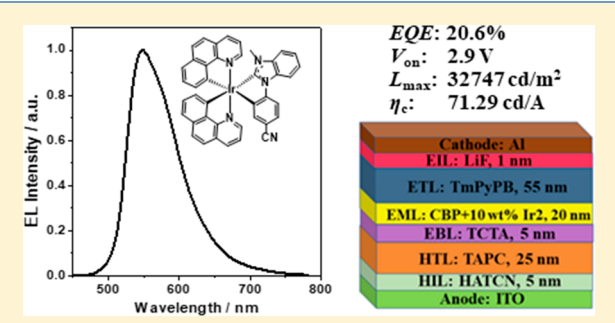
Inorganic Chemistry © Cite This: Inorg. Chem. XXXX, XXX, XXX–XXX

Neutral Cyclometalated Iridium(III) Complexes Bearing Substituted N-Heterocyclic Carbene (NHC) Ligands for High-Performance Yellow OLED Application

Bingqing Liu, *\binom{10}{0} Mohammed A. Jabed, *\binom{10}{0} Jiali Guo, *\binom{10}{0} Wan Xu, *\binom{1}{0} \binom{10}{0} Samuel L. Brown, *\binom{10}{0} Angel Ugrinov, *\binom{10}{0} Erik K. Hobbie, *\binom{10}{0} Svetlana Kilina, *\binom{10}{0} Anjun Qin, *\binom{10}{0} and Wenfang Sun**, *\binom{10}{0}

Supporting Information

ABSTRACT: The synthesis, crystal structure, and photophysics of a series of neutral cyclometalated iridium(III) complexes bearing substituted N-heterocyclic carbene (NHC) ancillary ligands $((C^N)_2Ir(R-NHC))$, where C^N and NHC refer to the cyclometalating ligand benzo[h]quinoline and 1-phenylbenzimidazole, respectively) are reported. The NHC ligands were substituted with electron-withdrawing or -donating groups on C4' of the phenyl ring $(R = NO_2 (Ir1), CN (Ir2), H (Ir3), OCH_3 (Ir4), N(CH_3)_2 (Ir5))$ or C5 of the benzimidazole ring $(R = NO_2 (Ir6), N(CH_3)_2 (Ir7))$. The configuration of Ir1 was confirmed by a single-crystal X-ray diffraction analysis. The ground- and excited-state properties of Ir1-



Ir7 were investigated by both spectroscopic methods and time-dependent density functional theory (TDDFT) calculations. All complexes possessed moderately strong structureless absorption bands at ca. 440 nm that originated from the C^N ligand based $^1\pi$, π^* / 1 CT (charge transfer)/ 1 d,d transitions and very weak spin—forbidden 3 MLCT (metal-to-ligand charge transfer)/ 3 LLCT (ligand-to-ligand charge transfer) transitions beyond 500 nm. Electron-withdrawing substituents caused a slight blue shift of the $^1\pi$, π^* / 1 CT/ 1 d,d band, while electron-donating substituents induced a red shift of this band in comparison to the unsubstituted complex Ir3. Except for the weakly emissive nitro-substituted complexes Ir1 and Ir6 that had much shorter lifetimes (\leq 160 ns), the other complexes are highly emissive in organic solutions with microsecond lifetimes at ca. 540–550 nm at room temperature, with the emitting states being predominantly assigned to $^3\pi$, π^* / 3 MLCT states. Although the effect of the substituents on the emission energy was insignificant, the effects on the emission quantum yields and lifetimes were drastic. All complexes also exhibited broad triplet excited-state absorption at 460–700 nm with similar spectral features, indicating the similar parentage of the lowest triplet excited states. The highly emissive Ir2 was used as a dopant for organic light-emitting diode (OLED) fabrication. The device displayed a yellow emission with a maximum current efficiency (η_c) of 71.29 cd A $^{-1}$, a maximum luminance (L_{max}) of 32747 cd m $^{-2}$, and a maximum external quantum efficiency (EQE) of 20.6%. These results suggest the potential of utilizing this type of neutral Ir(III) complex as an efficient yellow phosphorescent emitter.

■ INTRODUCTION

Cyclometalated iridium(III) complexes have drawn tremendous attention in the past three decades due to their facile synthesis and intriguing photophysical characteristics. To date, cyclometalated Ir(III) complexes have been explored for various applications, such as organic light-emitting diodes (OLEDs), 3,4 light-emitting electrochemical cells (LEECs), 5-7 photodynamic therapy (PDT), 8-10 nonlinear optics (NLO), 11-16 and luminescent biological labeling. Ty,18 Due to the strong spin-orbit coupling effect induced by the Ir(III) ion, nearly quantitative triplet excited-state formation quantum yield and phosphorescence efficiency can be obtained in some

cases. Consequently, phosphorescent Ir(III) complexes appear promising as robust emissive dopants for OLED fabrication. In addition, the emission properties of the Ir(III) complexes can be readily tuned by modification of the cyclometalating and/or ancillary ligands because the characteristics of the emitting triplet excited state depends strongly on the nature of the ligands.

N-heterocyclic carbenes (NHCs), a type of strong σ -donating species, have been widely employed as ligands for

Received: June 5, 2019



[†]Department of Chemistry and Biochemistry, North Dakota State University, Fargo, North Dakota 58108-6050, United States [‡]School of Materials Science and Engineering, South China University of Technology, Guangzhou 510640, People's Republic of China

[§]Engineering Research Center for Nanomaterials, Henan University, Kaifeng 475004, People's Republic of China Materials and Nanotechnology Program, North Dakota State University, Fargo, North Dakota 58108-6050, United States

organometallic complexes. 19-29 Because of the strong ligand field strength of NHCs, the metal-carbene antibonding orbitals lead to a high-lying lowest unoccupied molecular orbital (LUMO) in the formed complexes and consequently the emission energy is blue-shifted and the emission quantum yield improved.^{20–24} To date, investigations on organoiridium complexes containing NHC ligands have been primarily aimed toward OLED applications. 20-23 In the pioneering work reported by Thompson and co-workers, 20 two homoleptic neutral Ir(III) complexes with NHC ligands, i.e. fac-Ir(pmi)₃ (pmi = 1-phenyl-3-methylimidazolin-2-ylidene- $C_1C^{2\prime}$) and fac-Ir(pmb)₃ (pmb = 1-phenyl-3-methylbenzimidazolin-2-ylidene- $C_1C^{2\prime}$), showed higher emission energies but decreased photoluminescence (PL) efficiencies in comparison to the greenish emissive fac-Ir(ppy)₃ (ppy = 2-phenylpyridyl) and the sky blue emissive fac-Ir(F_2ppy)₃ ($F_2ppy = 2$ -(2,4difluorophenyl)pyridine) complexes. By replacing one NHC ligand with a diimine ligand, Kessler's group reported several cationic $Ir(N^{N})(NHC)_{2}^{+}$ complexes with yellow emission in neat films with PL efficiencies of up to 0.83.25

The seminal work on the development of heteroleptic (C^N)₂Ir(NHC) type of complexes was reported by Bielawski and co-workers, in which one NHC ligand and two cyclometalating 2-phenylpyridyl (C^N) ligands were employed.²⁷ This complex emitted at 497 nm in MeTHF with an emission yield of 19%. More recently, Zuo and co-workers²² reported a series of heteroleptic neutral (C^N)2Ir(NHC) complexes with various cyclometalating C^N and NHCs as the ligands. Among them, in the complexes with 2-(2,4difluorophenyl)pyridine (dfppy) as the cyclometalating C^N ligand and NHCs bearing electron-withdrawing -F or -CF3 substituents on the phenyl ring or NHCs with the phenyl ring being replaced with pyridine or pyrimidine rings, the emission was shifted to a bluer region. The blue-emitting OLED device utilizing $(dfppy)_2Ir(CF_3-pmi)$ $(CF_3-pmi) = 1-(3-trifluorome$ thylphenyl)-3-methylimidazole) as the dopant gave a maximum current efficiency of 37.83 cd A⁻¹, an external quantum efficiency of 10.3%, and a maximum luminance of 8709 cd $m^{-2}. \\$

Although the obstacles of synthesis have been solved, further exploration of the $(C^N)_2Ir(NHC)$ -type Ir(III) complexes remains dormant. Because of the promising applications of these types of complexes in OLEDs, we designed and synthesized seven $(C^N)_2Ir(NHC)$ -type Ir(III) complexes $(Ir1-Ir7, Chart\ 1)$ with different electron-donating $(-OCH_3)$ or $-N(CH_3)_2)$ or -withdrawing $(-NO_2 \text{ or } -CN)$ substituents on C5 of the benzimidazole or C4' of the phenyl rings at the NHC ligand (i.e., 3-methyl-1-(4-nitrophenyl)benzimidazol-3-ium iodide (L1), 1-(4-cyanophenyl)-3-methylbenzimidazol-3-

Chart 1. Chemical Structures of $(C^N)_2Ir(NHC)$ Complexes Ir1-Ir7

$$\begin{array}{c} R_2 \\ \text{(C5)} \\ \text{Ir1: } R_1 = \text{NO}_2, \, R_2 = \text{H} \\ \text{Ir2: } R_1 = \text{CN, } R_2 = \text{H} \\ \text{Ir3: } R_1 = \text{H, } R_2 = \text{H} \\ \text{Ir4: } R_1 = \text{OMe, } R_2 = \text{H} \\ \text{Ir5: } R_1 = \text{N(Me)}_2, \, R_2 = \text{H} \\ \text{Ir6: } R_1 = \text{H, } R_2 = \text{NO}_2 \\ \text{Ir7: } R_1 = \text{H, } R_2 = \text{N(Me)}_2 \end{array}$$

ium iodide (L2), 3-methyl-1-phenylbenzimidazol-3-ium iodide (L3), 1-(4-methoxyphenyl)-3-methylbenzimidazol-3-ium iodide (L4), 1-(4-dimethylaminophenyl)-3-methylbenzimidazol-3-ium iodide (L5), 5-nitro-3-methyl-1-phenylbenzimidazol-3-ium iodide (L6), and 5-dimethylamino-3-methyl-1-phenylbenzimidazol-3-ium iodide (L7)) and benzo[h]-quinoline as the C^N ligand. Selection of benzo[h]-quinoline as the C^N ligand was due to its rigidity that may potentially reduce the nonradiative decay rates. Different electron-donating or -withdrawing substituents were introduced to the NHC ligand in order to understand the effect of the substituents at the NHC ligand on the photophysics of these (C^N)_2Ir(NHC)-type complexes. The structure of Ir1 was determined by X-ray crystallography to confirm the configuration of these types of Ir(III) complexes.

EXPERIMENTAL SECTION

Synthesis and Characterizations. All chemicals and solvents were obtained from commercial sources and used as received without further purification. Silica gels (60 Å, 230–400 mesh) for column chromatography were purchased from Sorbent Technology. The precursor compounds 1 (1-(4-nitrophenyl)benzimidazole), 30 2 (1-(4-cyanophenyl)benzimidazole), 31 3 (1-phenylbenzimidazole), 30 and 4 (1-(4-methoxyphenyl)benzimidazole) 30 were prepared according to the reported procedures (see Scheme 1 for the synthetic route). The C^N ligand benzo[h]quinoline was purchased from Alfa-Aesar, and its Ir dimer [Ir(benzo[h]quinolone) $_2(\mu$ -Cl)] $_2$ was prepared by following the reported method. The synthetic schemes for the Ir(III) complexes Ir1–Ir7 are provided in Scheme 1. The synthetic details for the precursor compounds 5–7, the ligands L1–L7, and the complexes Ir1–Ir7, as well as the characterization data, are reported below.

The structures of the ligands L1–L7 were characterized by ¹H NMR spectroscopy, and the complexes Ir1–Ir7 were characterized by ¹H NMR, electrospray ionization mass spectrometry (ESI–HRMS), and elemental analyses. In addition, the configuration of complex Ir1 was determined by single-crystal X-ray crystallography. The ¹H NMR spectra were recorded on a Varian Oxford-400/Bruker-400 spectrometer in deuterated solvents (i.e. CDCl₃ or DMSO-d₆) using tetramethylsilane (TMS) as the internal standard. A Waters Synapt G2-Si mass spectrometer was used for the mass analyses. Elemental analyses were carried out by NuMega Resonance Laboratories, Inc. in San Diego, CA, USA. A Kappa Apex II Duo X-ray diffractometer was used to collect the X-ray diffraction (XRD) pattern of complex Ir1.

1-(4-Dimethylaminophenyl)benzimidazole (Compound 5). In a two-neck flask, 4-bromo-N,N-dimethylbenzenamine (2.00 g, 10 mmol), benzimidazole (1.18 g, 10 mmol), CuI (318 mg, 1.67 mmol), L-proline (383 mg, 3.33 mmol), and K_2CO_3 (2.76 g, 20 mmol) were mixed in 15 mL of DMSO and degassed with nitrogen for 30 min. The resulting mixture was heated to 130 °C for 24 h before it was partitioned between water and ethyl acetate. The organic layer was washed with brine, dried over Na_2SO_4 , and concentrated in vacuo. The crude product was then loaded on a silica gel column and eluted with ethyl acetate/hexane (v/v 1/1) to afford the product as a yellow solid (960 mg, 40%). 1H NMR (400 MHz, CDCl₃): δ 8.03 (s, 1H), 7.86 (dd, J = 6.0, 3.1 Hz, 1H), 7.45 (dd, J = 5.9, 3.3 Hz, 1H), 7.38–7.27 (m, 4H), 6.85 (d, J = 3.4 Hz, 1H), 6.82 (d, J = 3.3 Hz, 1H), 3.04 (s, 6H).

2,4-Dinitro-N-phenylbenzenamine (Compound a). A mixture of 2,4-dinitrochlorobenzene (4.05 g, 20 mmol), aniline (2.05 g, 22 mmol), and sodium acetate (1.64 g, 20 mmol) was dissolved in ethanol (10 mL) and heated to refluxed for 1 h. After the mixture was cooled to room temperature, the precipitated red-orange crystals were filtered out, washed with ethanol twice (10 mL each), and dried in vacuo to afford compound a as a red solid (4.70 g, 91%). ¹H NMR (500 MHz, CDCl₃): δ 9.98 (br, 1H), 9.19 (d, J = 2.6 Hz, 1H), 8.17 (dd, J = 9.5, 2.6 Hz, 1H), 7.51 (t, J = 7.8 Hz, 2H), 7.39 (t, J = 7.5 Hz, 1H), 7.31 (d, J = 7.8 Hz, 2H), 7.17 (d, J = 9.5 Hz, 1H).

Scheme 1. Synthetic Routes for Complexes Ir1-Ir7

L1/Ir1: R_1 = -NO₂, R_2 = -H; L2/Ir2: R_1 = -CN, R_2 = -H; L3/Ir3: R_1 = R_2 = -H;

L4/Ir4: R_1 = -OMe, R_2 = -H; L5/Ir5: R_1 = -NMe₂, R_2 = -H; L6/Ir6: R_1 = -H, R_2 = -NO₂; L7/Ir7: R_1 = -H, R_2 = -NMe₂

4-Nitro-N¹-phenyl-1,2-benzenediamine (Compound b). A suspension of compound a (4.70 g, 18.1 mmol) in alcohol (30 mL) was added to a solution of Na₂S (2.82 g, 36.2 mmol) and sulfur powder (1.15 g, 36.2 mmol) in water (30 mL). The mixture was heated to reflux for 2 h, diluted with water (30 mL), and cooled to room temperature. The obtained precipitate was filtered out and washed with warm water to give dark brown crystals of the title compound (4.10 g, 99%). ¹H NMR (400 MHz, CDCl₃): δ 7.77–7.64 (m, 2H), 7.35 (t, J = 7.8 Hz, 2H), 7.15 (d, J = 8.9 Hz, 1H), 7.12–6.97 (m, 3H), 5.76 (br, 1H), 3.70 (br, 2H).

5-Nitro-1-phenylbenzimidazole (Compound 6). A mixture of compound **b** (687 mg, 3 mmol) and formic acid (50 mL) was stirred at 100 °C for 12 h. Then, the reaction mixture was cooled to room temperature and concentrated in vacuo to afford a solid. The crude solid was partitioned between ethyl acetate (250 mL) and 30% ammonium hydroxide (25 mL). The organic layer was collected and concentrated in vacuo to afford compound **6** as an orange solid (710 mg, 99%). ¹H NMR (400 MHz, CDCl₃): δ 8.83 (d, J = 2.1 Hz, 1H), 8.33–8.26 (m, 2H), 7.67 (t, J = 7.7 Hz, 2H), 7.63–7.57 (m, 2H), 7.57–7.51 (m, 2H).

1-Phenylbenzimidazol-5-amine (Compound 7). Compound 6 (239 mg, 1 mmol) was dissolved in 10 mL of ethanol/water (v/v 4/1). Then, sodium dithionite (1.74 g, 10 mmol) was added to the solution and the resulting mixture was heated to reflux for 4 h. The reaction mixture was diluted with ethyl acetate and washed with water. The water layer was extracted several times with ethyl acetate. The organic layers were combined, dried over sodium sulfate, and concentrated to yield compound 7 as a white solid (200 mg, 96%). ¹H NMR (400 MHz, CDCl₃): δ 8.02 (s, 1H), 7.61–7.52 (m, 2H), 7.50 (t, J = 4.3 Hz, 2H), 7.44 (d, J = 7.3 Hz, 1H), 7.34 (d, J = 8.6 Hz, 1H), 7.16 (d, J = 2.0 Hz, 1H), 6.76 (dd, J = 8.6, 2.1 Hz, 1H), 3.35 (br, 2H).

General Synthetic Procedure for Ligands L1–L7. A mixture of 1 mmol of the corresponding precursor (compounds 1–7), 1.5 mmol of iodomethane (3 mmol for L7), and 10 mL of tetrahydrofuran was placed in a pressure tube with a Teflon cap and heated to 100 °C for 24 h. After the mixture was cooled to room

temperature, the resulting solid was filtered out, washed with tetrahydrofuran, and dried in vacuo.

- **L1.** A white solid was obtained as the target compound (358 mg, 94%). ¹H NMR (400 MHz, DMSO- d_6): δ 10.25 (s, 1H), 8.60 (d, J = 9.2 Hz, 2H), 8.18 (d, J = 7.6 Hz, 1H), 8.13 (d, J = 9.1 Hz, 2H), 7.97 7.90 (m, 1H), 7.85 7.68 (m, 2H), 4.20 (s, 3H).
- **L2.** A white solid was obtained as the target compound (336 mg, 93%). ¹H NMR (400 MHz, DMSO- d_6): δ 10.19 (d, J = 0.6 Hz, 1H), 8.33–8.23 (m, 2H), 8.21–8.12 (m, 1H), 8.05 (d, J = 8.5 Hz, 2H), 7.92 (dd, J = 8.2, 0.8 Hz, 1H), 7.84–7.67 (m, 2H), 4.18 (s, 3H).
- **L3.** A white solid was obtained as the target compound (218 mg, 65%). ¹H NMR (400 MHz, DMSO- d_6): δ 10.12 (s, 1H), 8.16 (d, J = 8.2 Hz, 1H), 7.87–7.68 (m, 8H), 4.17 (s, 3H).
- **L4.** A white solid was obtained as the target compound (245 mg, 67%). ¹H NMR (400 MHz, DMSO- d_6): δ 10.02 (s, 1H), 8.13 (d, J = 8.1 Hz, 1H), 7.80–7.66 (m, 5H), 7.28 (d, J = 8.9 Hz, 2H), 4.16 (s, 3H), 3.89 (s, 3H).
- **L5.** A white solid was obtained as the target compound (349 mg, 92%). ¹H NMR (400 MHz, DMSO- d_6): δ 9.95 (s, 1H), 8.12 (d, J = 8.1 Hz, 1H), 7.82–7.64 (m, 3H), 7.56 (d, J = 9.0 Hz, 2H), 6.96 (d, J = 9.0 Hz, 2H), 4.14 (s, 3H), 3.03 (s, 6H).
- **L6.** A yellow solid was obtained as the target compound (127 mg, 33%). ¹H NMR (400 MHz, DMSO- d_6): δ 10.40 (s, 1H), 9.21 (d, J = 2.1 Hz, 1H), 8.52 (dd, J = 9.2, 2.1 Hz, 1H), 8.06 (d, J = 9.2 Hz, 1H), 7.86–7.73 (m, 5H), 4.28 (s, 3H).
- **L7.** A white solid was obtained as the target compound (281 mg, 71%). ¹H NMR (400 MHz, DMSO- d_6): δ 9.83 (s, 1H), 7.80–7.68 (m, 5H), 7.62 (d, J = 9.2 Hz, 1H), 7.16 (dd, J = 9.3, 2.2 Hz, 1H), 7.12 (d, J = 2.1 Hz, 1H), 4.07 (s, 3H), 3.06 (s, 6H).

General Synthetic Procedure for Complexes Ir1–Ir7. The corresponding ligand L1–L7 (0.06 mmol), [Ir(benzo[h]-quinoline) $_2(\mu$ –Cl)] $_2$ (35 mg, 0.03 mmol), and Ag $_2$ O (28 mg, 0.12 mmol) were dissolved in 10 mL of 1,2-dichloroethane, and the reaction mixture was heated to reflux in the dark for 12 h (1 h for Ir6). The solution was then cooled to room temperature. After removal of the solvent under reduced pressure, purification by silica

gel column chromatography with dichloromethane and hexane (v/v 1/1) as eluent afforded a yellow solid as the target complex.

*Ir*1: 40 mg (yield: 83%). ¹H NMR (400 MHz, CDCl₃): δ 8.29 (d, J = 5.4 Hz, 1H), 8.24 (d, J = 5.4 Hz, 1H), 8.19 (d, J = 8.1 Hz, 1H), 8.09 (d, J = 8.0 Hz, 1H), 8.05 (d, J = 7.9 Hz, 1H), 7.96−7.87 (m, 2H), 7.80 (d, J = 6.4 Hz, 1H), 7.78 (d, J = 6.4 Hz, 1H), 7.62−7.48 (m, 3H), 7.46−7.39 (m, 2H), 7.38−7.31 (m, 2H), 7.28 (s, 1H), 7.24−7.04 (m, 4H), 6.71 (d, J = 6.8 Hz, 1H), 6.35 (d, J = 7.1 Hz, 1H), 3.28 (s, 3H). ESI-HRMS (m/z): calcd for [C₄₀H₂₆N₅O₂Ir + H]⁺, 802.1796; found, 802.1772. Anal. Calcd for C₄₀H₂₆N₅O₂Ir: C, 59.99; H, 3.27; N, 8.74. Found: C, 59.96; H, 3.62; N, 8.73.

Ir2: 26 mg (yield: 56%). 1 H NMR (400 MHz, CDCl₃): δ 8.28 (d, J = 5.4 Hz, 1H), 8.26 (d, J = 5.5 Hz, 1H), 8.19 (d, J = 7.7 Hz, 1H), 8.11 (d, J = 8.0 Hz, 1H), 8.08 (d, J = 8.1 Hz, 1H), 7.92 (d, J = 8.3 Hz, 1H), 7.83 (d, J = 8.8 Hz, 1H), 7.80 (d, J = 8.7 Hz, 1H), 7.59 (d, J = 5.3 Hz, 1H), 7.56 (d, J = 5.2 Hz, 1H), 7.49−7.31 (m, 5H), 7.29 (s, 1H), 7.24−7.03 (m, 5H), 6.72 (d, J = 6.9 Hz, 1H), 6.32 (d, J = 7.1 Hz, 1H), 3.30 (s, 3H). ESI-HRMS (m/z): calcd for [C₄₁H₂₆N₅Ir + H]⁺, 782.1897; found, 782.1872. Anal. Calcd for C₄₁H₂₆N₅Ir: C, 63.06; H, 3.36; N, 8.97. Found: C, 63.32; H, 3.75; N, 8.89.

Ir3: 9 mg (yield: 20%). ¹H NMR (400 MHz, CDCl₃): δ 8.36 (d, J = 4.5 Hz, 1H), 8.30 (d, J = 4.7 Hz, 1H), 8.22 (d, J = 8.2 Hz, 1H), 8.04 (d, J = 7.8 Hz, 1H), 8.00 (d, J = 7.9 Hz, 1H), 7.89 (d, J = 7.8 Hz, 1H), 7.76 (d, J = 8.7 Hz, 2H), 7.54 (d, J = 8.8 Hz, 1H), 7.51 (d, J = 8.7 Hz, 1H), 7.40−7.31 (m, 3H), 7.28 (d, J = 8.1 Hz, 1H), 7.23 (d, J = 8.0 Hz, 1H), 7.17−7.00 (m, 5H), 6.81 (d, J = 5.7 Hz, 1H), 6.74 (t, J = 6.2 Hz, 2H), 6.37 (d, J = 7.0 Hz, 1H), 3.27 (s, 3H). ESI-HRMS (m/z): calcd for [C₄₀H₂₇N₄Ir + H]⁺, 757.1945; found, 757.1938. Anal. Calcd for C₄₀H₂₇N₄Ir·0.1CH₂Cl₂: C, 63.01; H, 3.59; N, 7.33. Found: C, 62.77; H, 3.30; N, 7.26.

Ir4: 10 mg (yield: 4%) (by scaling up all of the reagents and solvent to 5-fold of the scale described in the above general synthetic procedure). ¹H NMR (400 MHz, CDCl₃): δ 8.39 (d, J = 4.9 Hz, 1H), 8.30 (d, J = 5.7 Hz, 1H), 8.16 (d, J = 8.3 Hz, 1H), 8.03 (d, J = 7.1 Hz, 1H), 8.00 (d, J = 7.4 Hz, 1H), 7.80 (d, J = 8.7 Hz, 1H), 7.76 (d, J = 3.0 Hz, 1H), 7.74 (d, J = 3.2 Hz, 1H), 7.53 (d, J = 8.9 Hz, 1H), 7.50 (d, J = 8.7 Hz, 1H), 7.40−7.30 (m, 3H), 7.25−6.95 (m, 6H), 6.75 (d, J = 6.8 Hz, 1H), 6.55 (dd, J = 8.6, 2.9 Hz, 1H), 6.40 (d, J = 3.0 Hz, 1H), 6.37 (d, J = 7.0 Hz, 1H), 3.48 (s, 3H), 3.25 (s, 3H). ESI-HRMS (m/z): calcd for [C₄₁H₂₉N₄OIr·0.2CH₂Cl₂·0.1C₆H₁₄ (C₆H₁₄ = hexane): C, 61.87; H, 3.83; N, 6.90. Found: C, 62.10; H, 3.67; N, 6.51

Ir5: 10 mg (yield: 4%) (by scaling up all of the reagents and solvent to 5-fold of the scale described in the above general synthetic procedure). 1 H NMR (400 MHz, CDCl₃): δ 8.44 (d, J = 4.4 Hz, 1H), 8.32 (d, J = 5.5 Hz, 1H), 8.15 (d, J = 8.1 Hz, 1H), 8.02 (d, J = 8.0 Hz, 1H), 7.98 (d, J = 7.3 Hz, 1H), 7.82−7.70 (m, 3H), 7.53 (d, J = 8.8 Hz, 1H), 7.49 (d, J = 8.7 Hz, 1H), 7.34 (d, J = 7.9 Hz, 3H), 7.22 (d, J = 6.6 Hz, 2H), 7.17−7.09 (m, 3H), 7.06 (dd, J = 8.0, 5.4 Hz, 1H), 6.81 (d, J = 7.0 Hz, 1H), 6.49−6.36 (m, 2H), 6.32 (d, J = 2.9 Hz, 1H), 3.25 (s, 3H), 2.55 (s, 6H). ESI-HRMS (m/z): calcd for $C_{42}H_{32}N_5Ir$ + H] $^+$, 800.2367; found, 800.2333. Anal. Calcd for $C_{42}H_{32}N_5Ir$ ·0.1CH $_2$ Cl $_2$: C, 62.62; H, 4.02; N, 8.67. Found: C, 62.59; H, 3.85; N, 9.05.

Ir6: 23 mg (yield: 48%). 1 H NMR (400 MHz, CDCl₃): δ 8.48−8.22 (m, 4H), 8.19 (s, 1H), 8.10 (d, J = 7.8 Hz, 1H), 8.07 (d, J = 7.9 Hz, 1H), 7.89 (d, J = 7.9 Hz, 1H), 7.81 (d, J = 8.7 Hz, 2H), 7.58 (d, J = 8.8 Hz, 1H), 7.55 (d, J = 8.8 Hz, 1H), 7.41 (t, J = 8.2 Hz, 2H), 7.25−7.02 (m, 5H), 6.91−6.79 (m, 2H), 6.76 (d, J = 6.9 Hz, 1H), 6.33 (d, J = 6.8 Hz, 1H), 3.39 (s, 3H). ESI-HRMS (m/z): calcd for [C₄₀H₂₆N₅O₂Ir + H]⁺, 802.1796; found, 802.1785. Anal. Calcd. for C₄₀H₂₆N₅O₂Ir·0.1C₆H₁₄·3H₂O: C, 56.47; H, 3.90; N, 8.11. Found: C, 56.38; H, 4.20; N, 8.06.

Ir7: 19 mg (yield: 40%). ¹H NMR (400 MHz, CDCl₃): δ 8.39 (d, J = 5.4 Hz, 1H), 8.36 (d, J = 5.3 Hz, 1H), 8.07–8.00 (m, 2H), 7.83 (d, J = 7.7 Hz, 1H), 7.78 (d, J = 8.7 Hz, 2H), 7.55 (d, J = 8.7 Hz, 1H), 7.53 (d, J = 8.8 Hz, 1H), 7.39 (d, J = 7.7 Hz, 1H), 7.36 (d, J = 7.8 Hz, 1H), 7.23–6.99 (m, 6H), 6.89–6.72 (m, 4H), 6.47 (d, J = 2.1 Hz, 1H), 6.41 (d, J = 7.0 Hz, 1H), 3.22 (s, 3H), 3.00 (s, 6H). ESI-HRMS

(m/z): calcd for $[C_{42}H_{32}N_5Ir + H]^+$, 800.2367; found, 800.2357. Anal. Calcd for $C_{42}H_{32}N_5Ir \cdot 0.9C_6H_{14} \cdot 4H_2O$: C, 60.02; H, 5.59; N, 7.38. Found: C, 59.89; H, 5.98; N, 7.76.

Photophysical Studies. The solvents used for the photophysical studies are spectrophotometric grade and were purchased from Alfa Aesar Co., Inc. The ultraviolet-visible (UV-vis) absorption spectra of Ir1-Ir7 were recorded on a Varian Cary 50 spectrophotometer. The steady-state emission spectra of Ir1-Ir7 were collected on a HORIBA FluoroMax 4 fluorometer/phosphorometer. The absolute emission quantum yields (Φ_{em}) were determined via a fiber coupled Ocean Optics integrating sphere. A broad white light LED was used as the excitation light source, which was connected to a set of Delta linear-variable filters (LVFs) and then to the integrating sphere via a fiber. The excitation wavelength was narrowed and positioned at 450 nm using the LVFs. Ocean Optics UV-vis QE65000 and Ocean Optics NIRQ512 spectrometers were coupled through a bifurcated fiber to the integrating sphere, which provides an effective detection range from 350 to 1700 nm. Each sample solution was degassed and placed in an anaerobic environment prior to the measurement.

The nanosecond transient absorption (TA) spectra and decays, triplet excited-state quantum yields $(\Phi_{\rm T})$, and triplet lifetimes $(\tau_{\rm TA})$ were measured on the laser flash photolysis spectrometer (Edinburgh LP920) in the nitrogen-purged toluene solutions. The third harmonic output (355 nm) of a Quantel Brilliant Nd:YAG laser with 4.1 ns pulse duration and 1 Hz repetition rate was utilized as the excitation source. Each sample solution was purged with nitrogen for 40 min before the measurement. The triplet excited-state molar extinction coefficients $(\varepsilon_{\rm T})$ at the TA maxima were deduced using the singlet depletion method. To obtain the triplet quantum yields, the relative actinometry method was applied using a silicon naphthalocyanine (SiNc) in benzene solution $(\varepsilon_{\rm 590\,nm}=70000~{\rm L~mol}^{-1}~{\rm cm}^{-1},~\Phi_{\rm T}=0.2)^{35}$ as the reference.

DFT Calculations. All calculations were performed using the Gaussian16 software package.³⁶ The ground-state geometries of the complexes were optimized using density functional theory (DFT).³⁷ The long-range corrected functional CAM-B3LYP³⁸ was used with a mixed basis set of LANL2DZ³⁹ for Ir(III) and 6-31G*⁴⁰ for all other atoms. Solvent effects were incorporated in the calculations by using the conductor like polarizable continuum model (CPCM) reaction field method.⁴¹ Toluene was chosen as the solvent for consistency with the experimental studies.

A linear response time dependent DFT (TDDFT)⁴² methodology was adopted to calculate 70 excited states in toluene using the same functional and basis set as those used for the ground-state calculations. Although our previous joint experimental and computational studies demonstrated that the hybrid functional PBE0⁴³ was capable of accurately representing the excited properties of many Ir(III) complexes, 12,44 PBE0 failed in reproducing the correct trends for the complexes studied in this work, especially for complexes containing the nitro substituent. It has been discussed in the literature that long-range corrected functionals, such as CAM-B3LYP, more accurately describe the localization/delocalization properties of charge transfer states in the donor-acceptor molecules than hybrid functionals, despite the overall overestimation of the excited energies. 45,46 As such, we chose CAM-B3LYP for our calculations, while we applied a constant shift of -0.82 eV to correct the blue shift and align the calculated absorption spectra with the experimental spectra. To construct the absorption spectra, each optical transition obtained from TDDFT calculations was broadened by the Gaussian function with a width of $\sigma = 0.08$ eV, which well reproduces the thermal broadening of the experimental spectra.

Emission energies were calculated by the Δ SCF method. The triplet ground-state geometry was optimized (using the CAM-B3LYP functional and LAN2DS/6-31G* basis set) and then used for TDDFT calculations of the vertical triplet excitations.

To better understand the nature of the excited states, natural transition orbitals (NTOs)⁵⁰ were calculated. NTOs are compact representations of the density of the excited electron—hole pair using diagonalized transition density matrices obtained from the TDDFT

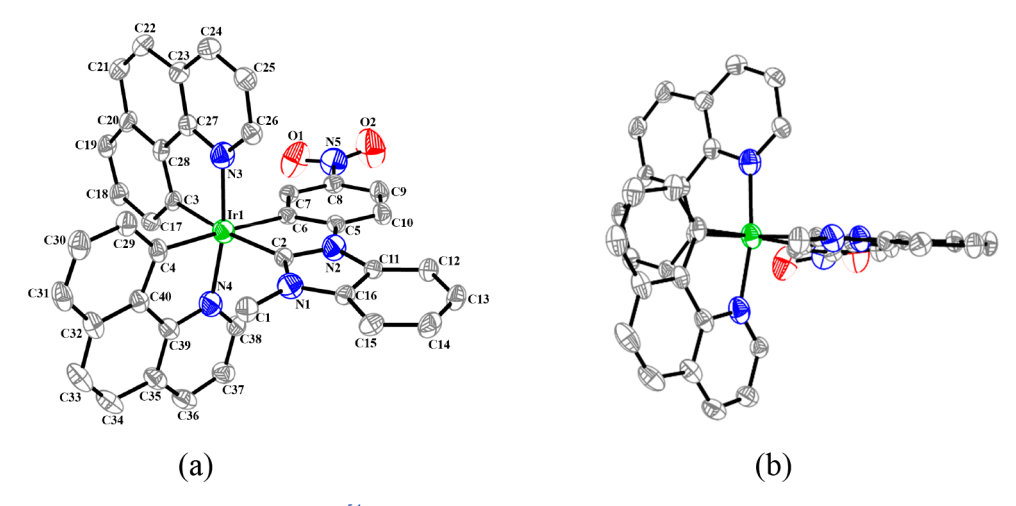


Figure 1. ORTEP (Oak Ridge Thermal Ellipsoid Plot)⁵⁴ diagram displaying thermal ellipsoids at the 50% probability level and atom labels for **Ir1**. Hydrogen atoms are omitted for clarity. (a) and (b) are viewed from different angles.

calculations. All NTOs were visualized by VMD⁵¹ code using 0.02 isosurface resolution.

X-ray Crystallography. The single crystal of Ir1 was grown by slow diffusion of hexane into a dilute dichloromethane solution of Ir1. The crystallographic data were collected on a Bruker Kappa Apex II Duo X-ray diffractometer with an Apex 2 CCD area detector at 200.01 K. The structure was solved with the ShelXT⁵² structure solution program embedded in Olex2, 33 using Intrinsic Phasing, and refined with the ShelXL refinement package with least-squares minimization.

Fabrication and Characterization of the OLEDs. The multilayer OLEDs were fabricated by the vacuum-deposition method. The 95 nm indium tin oxide (ITO) coated glass substrates with a sheet resistance of 15–20 Ω sq⁻¹ were subjected to a routine cleaning process of acetone, isopropyl alcohol, detergent, deionized water, and isopropyl alcohol in an ultrasonic bath and treated with O2 plasma for 10 min. Organic layers and the cathode were sequentially deposited on the ITO-coated glass substrates by thermal evaporation under high vacuum ($<5 \times 10^{-4}$ Pa). The deposition rates were 1.0 Å s⁻¹ for organic layers, 0.1 Å s⁻¹ for the LiF layer, and 3-5 Å s⁻¹ for the Al cathode, respectively. The active area of each device was 9 mm². The electroluminescence spectra (EL), the current density-voltage characteristics (J-V), and the current density-voltage-luminance curves (J-V-L) of the OLEDs were detected on a Photo Research SpectraScan PR-745 spectroradiometer and a Keithley 2450 source meter, and the data were recorded simultaneously. All device characterization was carried out at room temperature under ambient laboratory conditions. The device configuration is ITO/HATCN (5 nm)/TAPC (25 nm)/TCTA (5 nm)/CBP:10 wt % Ir2 (20 nm)/ TmPyPB (55 nm)/LiF (1 nm)/Al, where 1,4,5,8,9,11-hexaazatriphenylenehexacarbonitrile (HATCN) is the hole injection layer (HIL), 1bis[4-[N,N-di-4-tolylamino]phenyl]cyclohexane (TAPC) works as the hole-transporting layer (HTL), tris(4-carbazoyl-9-ylphenyl)amine (TCTA) serves as the electron-blocking layer (EBL), 4,4'-bis(9Hcarbazol-9-yl)-1,1'-biphenyl (CBP) functions as the host, 1,3,5-tris(mpyrid-3-ylphenyl)benzene (TmPyPB) acts as the electron-transporting layer (ETL) and the hole-blocking layer (HBL), and LiF is the electron injection layer (EIL). The molecular structures of HATCN, TAPC, TCTA, CBP, and TmPyPB are shown in Figure S1 in the Supporting Information.

RESULTS AND DISCUSSION

Single-Crystal Structure of Ir1. A suitable single crystal of **Ir1** for X-ray crystallographic analysis was obtained by slow diffusion of hexane into a dilute dichloromethane solution of **Ir1** at room temperature. The crystal structure of **Ir1** was determined by X-ray diffraction at 200.01 K, and the obtained

Table 1. Selected Bond Lengths (Å) and Angles (deg) for Irl

Ir1-N3	2.059(5)	Ir1-C3	2.059(5)
Ir1-N4	2.061(5)	Ir1-C4	2.073(6)
Ir1-C2	2.054(5)	Ir1-C6	2.086(6)
N4-Ir1-C4	80.6(2)	C2-Ir1-C3	171.9(2)
N4-Ir1-C6	97.3(2)	C2-Ir1-C4	101.6(2)
N3-Ir1-N4	169.6(19)	C2-Ir1-C6	77.7(2)
N3-Ir1-C3	80.1(2)	C3-Ir1-N4	92.0(2)
N3-Ir1-C4	92.2(2)	C3-Ir1-C4	86.2(2)
N3-Ir1-C6	89.9(2)	C3-Ir1-C6	94.6(2)
C2-Ir1-N4	91.5(2)	C4-Ir1-C6	177.8(2)
C2-Ir1-N3	97.3(2)		

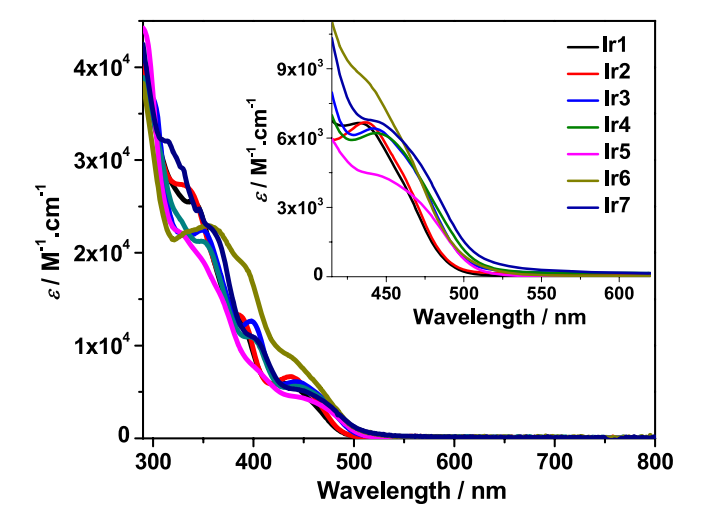


Figure 2. Experimental UV—vis absorption spectra of complexes **Ir1**—**Ir7** at room temperature in toluene. The inset is the expansion of the spectra in the region of 415–620 nm.

crystallographic data are compiled in Table S1 in the Supporting Information.

Figure 1 shows the top-down and side views of the crystal structure for Ir1. The selected bond lengths and bond angles around the Ir(III) center are presented in Table 1. The crystal structure clearly indicates that the N atoms on the C^N ligands coordinate to the metal center in a trans configuration with a

Table 2. Photophysical Properties of Complexes Ir1-Ir7

	$\lambda_{\rm abs}/{ m nm} \; (\log arepsilon)^a$	$\begin{array}{c} \lambda_{\rm em}/{ m nm} \; (au_{ m em}/{ m ns}); \ \Phi_{ m em} \; ({ m room \; temp}) \end{array}$	$k_{\rm r}/{\rm s}^{-1}$	$k_{\rm nr}/{\rm s}^{-1}$	$\frac{\lambda_{\rm em}/{\rm nm}^d}{(77 \text{ K})}$	$\lambda_{\text{T1-Tn}}/\text{nm} \ (au_{\text{TA}}/\text{ns, log } arepsilon_{\text{T1-Tn}}); \ \Phi_{\text{T}}^{\ e}$
Ir1	290 (4.60), 340 (4.41), 386 (4.11), 433 (3.82)	544 (45); 0.0027	2.40×10^{5}	8.86×10^{7}	_f	532 (50, -); - ^g
Ir2	290 (4.59), 330 (4.44), 387 (4.12), 436 (3.82)	540 (5300); 0.16	1.21×10^5	6.34×10^5	522, 560, 608 (sh.)	502 (5700, -); - ^g
Ir3	290 (4.57), 349 (4.35), 398 (4.11), 442 (3.81)	554 (3520); 0.15	1.85×10^5	1.05×10^6	531, 568, 617 (sh.)	547 (4050, 4.45); 0.23
Ir4	290 (4.59), 349 (4.33), 397 (4.04), 444 (3.79)	549 (2640); 0.064	1.28×10^5	1.87×10^6	519, 551, 597 (sh.)	547 (2430, 4.53); 0.19
Ir5	290 (4.65), 326 (4.35), 391 (3.94), 445 (3.64)	552 (2490); 0.046	1.15×10^{5}	2.39×10^{6}	524, 554	550 (2550, 4.57); 0.16
Ir6	290 (4.63), 354 (4.41), 390 (4.27), 433 (3.94)	545 (160); 0.016	3.33×10^{5}	2.05×10^{7}	528, 566	523 (160, 4.37); 0.30
Ir7	290 (4.63), 315 (4.51), 355 (4.37), 400 (4.05), 443 (3.72)	552 (4030); 0.088	7.04×10^4	7.30×10^{5}	534, 569	540 (4000, 4.20); 0.31

^aElectronic absorption band maxima (λ_{abs}) and molar extinction coefficients (log ε) in toluene at room temperature. ^bRoom-temperature emission band maxima (λ_{em}) and lifetimes (τ_{em}) for Ir1–Ir7 in toluene at a concentration of 1 × 10⁻⁵ mol L⁻¹. The absolute quantum yields were measured via the Ocean Optics integrating sphere $(\lambda_{ex} = 450 \text{ nm})$. The emission signals were integrated in the range of 350–820 nm. ^cRadiative (k_r) and nonradiative decay rates (k_{nr}) in toluene calculated by $k_r = \Phi_{em}/(\Phi_T\tau_{em})$ and $k_{nr} = (1 - \Phi_{em})/(\Phi_T\tau_{em})$, respectively. For Ir3–Ir7, the estimated triplet quantum yields (Φ_T) from the transient absorption measurement were used. For Ir1 and Ir2, Φ_T was assumed to be 0.25. ^dEmission band maxima in MTHF glassy matrix at 77 K. ^eNanosecond TA band maxima (λ_{T1-Tp}) , triplet excited-state lifetimes (τ_{TA}) , molar extinction coefficients (ε_{T1-Tn}) , and quantum yields (Φ_T) measured in toluene at room temperature. The emission signal was too weak to be recorded. ^gDue to the lack of a bleaching band, the ε_{T1-Tn} values were unable to be estimated by the singlet depletion method. Consequently, the Φ_T values could not be calculated.

bond angle of 169.6°, which is slightly distorted from the octahedral geometry. The other bond angles around the Ir(III) center also deviate from the angles for an ideal octahedral geometry. In comparison with the Ir(III) complex bearing 1methyl-3-phenylbenzimidazolylidene and 2-phenylpyridine ligands, ²² similar bond angles and bond lengths were found. The Ir-C2 and Ir-C6 bonds in Ir1 were 0.010 and 0.025 Å shorter than the corresponding bonds in the reported complex, while slightly longer Ir-N3 and Ir-N4 bonds of 0.005 and 0.008 Å, respectively, were found in Ir1 in comparison to those in the reported complex. These minor differences are likely due to the rigidity of the cyclometalating benzo [h] quinoline ligands. Complexation of the NHC ligand with the metal center prohibited the rotation of the N-phenyl substituent, resulting in a nearly coplanar configuration (7.80°) between the phenyl ring and the benzimidazole moiety (Figure S2 in the Supporting Information).

Electronic Absorption. The electronic absorption spectra of complexes Ir1-Ir7 were measured in toluene, dichloromethane, tetrahydrofuran, and acetonitrile. The spectra in toluene are displayed in Figure 2, and the absorption band maxima and molar extinction coefficients are compiled in Table 2. The normalized absorption spectra in the other solvents are presented in Figure S3 in the Supporting Information. The concentration-dependence study from 5 × 10^{-6} to 1×10^{-4} mol L⁻¹ showed that the absorption of these complexes in toluene obeyed Beer's law without forming ground-state aggregates. All complexes possessed intense absorption bands ($\varepsilon \approx 10^4 \text{ L mol}^{-1} \text{ cm}^{-1}$) in the wavelength range of 290–420 nm and a broader and weaker band ($\varepsilon \approx 10^3$ L mol⁻¹ cm⁻¹) at 420-500 nm. Taking into account the spectral features and the molar extinction coefficients, we tentatively assign the 290-420 nm bands predominantly to spin-allowed ligand-localized ${}^1\pi$, π^* transitions. For the 420– 500 nm band, the structureless feature suggests charge transfer transitions. However, the moderate molar extinction coefficient implies significant contributions of the $^{1}\pi_{0}\pi^{*}$ transitions. Attribution of the major absorption bands, including the absorption band centered at 433-445 nm, to predominant $^{1}\pi,\pi^{*}$ transitions is supported by the minor solvatochromic

effect of these complexes in solvents with varied polarities, which is a characteristic of ${}^{1}\pi,\pi^{*}$ transitions (see Figure S3 in the Supporting Information). These assignments are also confirmed by the TDDFT calculations that will be discussed in the following paragraph. In addition, all complexes exhibited very weak absorption tails beyond 500 nm. With reference to the other reported Ir(III) complexes with NHC ligands, 22 we attribute this tail to spin-forbidden charge transfer transitions (3 MLCT/ 3 LLCT).

To better understand the natures of the electronic transitions, TDDFT calculations were carried out for complexes Ir1-Ir7 in toluene. The spectral features and the trend of the calculated spectra matched the experimental spectra very well (Figures S4 and S5 in the Supporting Information). The natural transition orbitals (NTOs) for the electrons and holes corresponding to the lowest-energy electronic transitions are provided in Table 3, and the NTOs corresponding to the transitions contributing to the highenergy major absorption bands are provided in Tables S2 and S3 in the Supporting Information. As the NTOs in Table 3 show, the predominant contributors to the low-energy absorption band at ca. 440 nm are the C^N ligand-localized $^{1}\pi,\pi^{*}$ transition, admixing with a 1 MLCT (metal-to-ligand charge transfer) transition. In addition, ¹LLCT (ligand-toligand charge transfer), ¹LMCT (ligand-to-metal charge transfer), and ¹d,d transitions also made minor contributions. The NTOs indicate that the NHC ligand essentially is not involved in the low-energy transitions. Therefore, introducing electron-donating or -withdrawing substituents to the NHC ligand has a minor effect on the low-energy absorption band at ca. 440 nm. Nevertheless, electron-donating substituents, such as OCH₃ and N(CH₃)₂ groups, induced a slight red shift of the low-energy absorption band in Ir4, Ir5, and Ir7 regardless of whether the substituent was introduced at the phenyl ring or at the benzimidazole motif. In contrast, electron-withdrawing substituents, such as CN and NO2 groups, caused a slight blue shift of the low-energy absorption band in Ir1, Ir2, and Ir6.

The NTOs in Table S2 in the Supporting Information show that the transitions in the region of 380–425 nm have predominant $^1\pi$, $\pi^*/^1$ LLCT/ 1 MLCT characters, with the

Table 3. NTOs of the Holes and Electrons for the Low-Energy Transitions in Ir1–Ir7, Calculated by the TDDFT Method with the CAM-B3LYP Functional and LANL2DZ/6-31G* Basis Set in Toluene

	ted states properties	Hole	Electron	Exci and	ted states properties	Hole	Electron
Ir1	S_1 444 nm $f = 0.155$			Ir5	S_1 451 nm $f = 0.136$		
	S_2 440 nm $f = 0.029$				S_2 446 nm $f = 0.024$		
Ir2	S_1 444 nm $f = 0.154$			Ir6	S_1 445 nm $f = 0.153$		
	S_2 440 nm $f = 0.030$				S_2 440 nm $f = 0.021$		
Ir3	S_1 449 nm $f = 0.144$			Ir7	S_1 452 nm $f = 0.139$		
	S_2 445 nm $f = 0.025$				S_2 447 nm $f = 0.023$		
Ir4	S_1 449 nm $f = 0.144$						
	S_2 445 nm $f = 0.025$						

contribution from the 1 LLCT ($\pi(\text{NHC}) \rightarrow \pi^{*}(\text{C}^{\wedge}\text{N})$) transition becoming more significant. Similar to the case for the lowest-energy absorption band at ca. 440 nm, electron-donating substituents caused a red shift of the 380–425 nm band while electron-withdrawing substituents induced a blue shift. For the high-energy absorption bands at <380 nm, they are also composed of mixed $^{1}\pi,\pi^{*}/^{1}\text{CT}/^{1}\text{d},\text{d}$ transitions, with the holes or electrons becoming more delocalized and thus the oscillator strengths being increased.

Photoluminescence. The emission of complexes Ir1–Ir7 was studied in different solvents at room temperature. The emission spectra in deaerated toluene are displayed in Figure 3, and the emission parameters, i.e. the emission quantum yields $(\tau_{\rm em})$ and lifetimes $(\Phi_{\rm em})$, are given in Table 2. All complexes exhibited long-lived (several microseconds except for Ir1 and Ir6) and oxygen-sensitive bright yellow luminescence with large red shifts in comparison to their corresponding excitation wavelength, suggesting the phosphorescent nature of the

emission. The normalized emission spectra and the emission characteristics in other solvents are provided in Figure S6 and Table S4 in the Supporting Information, respectively. Comparison of the experimental and calculated emission energies of Ir1-Ir7 in toluene is provided in Figure S7 in the Supporting Information. The emission spectra for all complexes are broad and featureless, indicative of chargetransfer characters. On the other hand, the emission energies in all solvents are quite similar, which is a characteristic of ${}^3\pi$, π * emission. Moreover, the emission energies of all complexes resemble each other, suggesting the similar nature of the emitting states. However, the longer lifetimes of Ir2 in comparison to those of the other complexes in each corresponding solvent along with the clearer vibronic structure in toluene imply a somewhat larger contribution of the $^3\pi$, π * character in the emitting state of Ir2.

The NTOs in Table 4 indicate that the holes of the T_1 states in all complexes are delocalized on one of the C^{\wedge}N ligands and

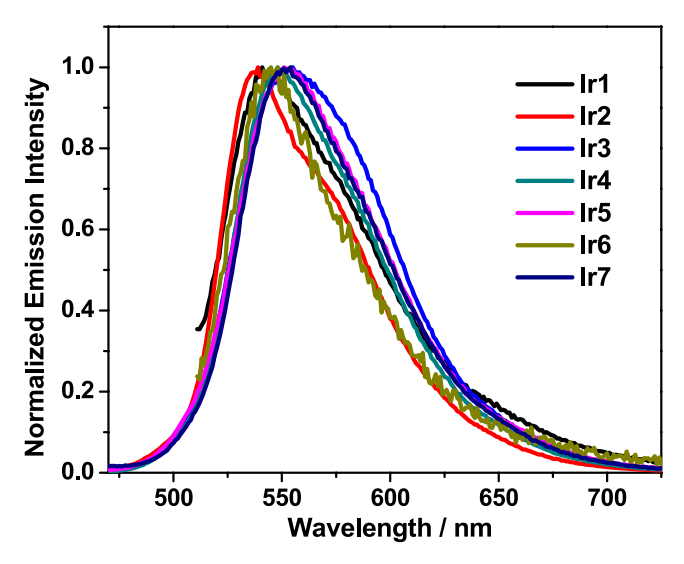


Figure 3. Experimental emission spectra of complexes Ir1 ($\lambda_{\rm ex}$ = 434 nm), Ir2 ($\lambda_{\rm ex}$ = 437 nm), Ir3 ($\lambda_{\rm ex}$ = 442 nm), Ir4 ($\lambda_{\rm ex}$ = 444 nm), Ir5 ($\lambda_{\rm ex}$ = 445 nm), Ir6 ($\lambda_{\rm ex}$ = 433 nm), and Ir7 ($\lambda_{\rm ex}$ = 444 nm) in deoxygenated toluene at room temperature.

Table 4. NTOs Contributing to the T_1 States of Complexes Ir1–Ir7 in Toluene, Calculated by the Δ SCF-TDDFT Method Using the CAM-B3LYP Functional and LANL2DZ/6-31G* Basis Set

	T ₁ Energy (nm) ^a	Hole	Electron		T ₁ Energy (nm) ^a	Hole	Electron
Ir1	545	***		Ir5	548		
Ir2	545			Ir6	545		
Ir3	546			Ir7	548	基础	群
Ir4	547	XXXXX	X Y X				

^aThe emission energies were calculated by Δ SCF method.

the d orbital of the Ir(III) ions, while the electrons are mainly distributed on the same C^N ligand. Therefore, the emission of these complexes predominantly emanates from the ${}^3\pi,\pi^*/{}^3\text{MLCT}$ (d(Ir) $\to\pi^*(\text{C^N})$) states.

To further confirm the nature of the emitting states in Ir1-Ir7, emission of these complexes in a glassy matrix of 2methyltetrahydrofuran (MTHF) at 77 K was studied and the emission band maxima are given in Table 2. A comparison of the emission spectrum of each complex (except for Ir1, in which the emission at 77 K was too weak to be monitored) in fluid MTHF solution at room temperature and in an MTHF glassy matrix at 77 K is provided in Figure S8 in the Supporting Information. The emission spectra of these complexes at 77 K were all blue-shifted and became structured. The vibronic progressions were in the range of 1033-1410 cm⁻¹, which are in line with the ring stretching modes of the aromatic rings. In addition, the thermally induced Stokes shifts for these complexes were in the range of 489–836 cm⁻¹. These features are consistent with the predominant ${}^{3}\pi_{,}\pi^{*}/{}^{3}MLCT$ nature of the emitting states in these complexes.

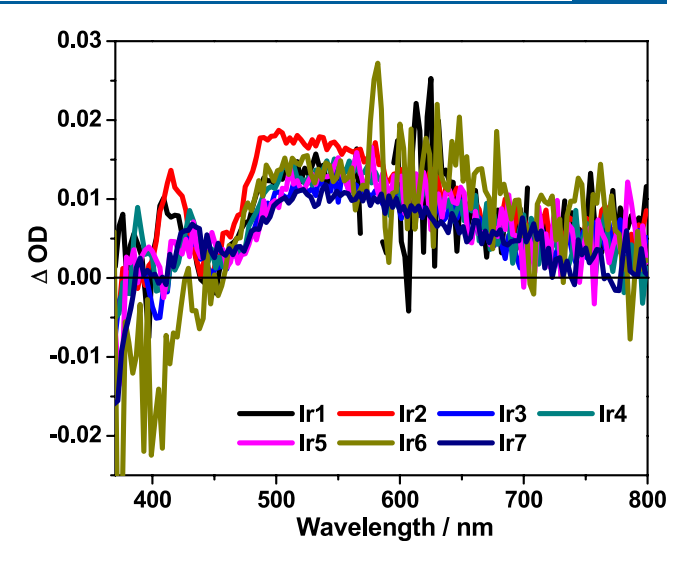


Figure 4. Nanosecond transient absorption spectra of complexes Ir1–Ir7 in deaerated toluene immediately after 355 nm excitation ($A_{355 \text{ nm}} = 0.4$ in a 1 cm cuvette).

Table 5. Summary of the Ir2-Based OLED Performance

$V_{\text{on}} (V)^a$	$L \left(cd/m^2 \right)^b$	$\eta_{\rm C} ({\rm cd/A})^{b}$	$\eta_{\rm P} ({\rm lm/W})^{b}$	EQE (%) ^b
2.9	32747	71.29	68.90	20.6

 $^aV_{\rm on}$ is the turn-on voltage at 1 cd/m². b The luminance (L), current efficiency ($\eta_{\rm c}$), power efficiency ($\eta_{\rm P}$), and EQE are the maximum values of the device.

Although the emission energies and natures for these complexes are similar and the NHC ligand is not involved in the emitting state, the substituents on the NHC ligand still exerted minor effects on the emission energies. Electronwithdrawing substituents caused a slight blue shift of the emission bands in Ir1, Ir2, and Ir6 in comparison to that in Ir3, while electron-donating substituents had a negligible effect on the emission energies of Ir4, Ir5, and Ir7. In contrast, the effects of the substituents at the NHC ligand on the emission lifetimes and quantum yields are drastic. An examination of the emission parameters given in Table 2 and Table S4 in the Supporting Information found that complexes Ir1 and Ir6, which contain the strongly electron-withdrawing nitro substituent, exhibited much shorter emission lifetimes and much weaker emission in comparison to those of the other complexes regardless of the solvent used. While the electrondonating substituents OCH₃ and N(CH₃)₂ also reduced the emission lifetimes and quantum yields in Ir4, Ir5, and Ir7 with respect to those in Ir3, the reductions were generally more pronounced in Ir5 and Ir7, which contain the more strongly electron-donating substituent $N(CH_3)_2$. Interestingly, the longest emission lifetime and strongest emission were found in Ir2, which bears an electron-withdrawing CN substituent.

The effects of the substituents on the emission lifetimes and quantum yields can be rationalized by the different influences of the substituent on the radiative decay rate constant $(k_{\rm r})$ and nonradiative decay rate constants $(k_{\rm nr})$ for these complexes. The $k_{\rm r}$ and $k_{\rm nr}$ data given in Table 2 indicate that the different substituents at the NHC ligand do not change the $k_{\rm r}$ values significantly (~4.7-fold), while they alter the $k_{\rm nr}$ values by approximately 140-fold. The CN-substituted complex Ir2 possesses the lowest $k_{\rm nr}$ value but a comparable $k_{\rm r}$ value with

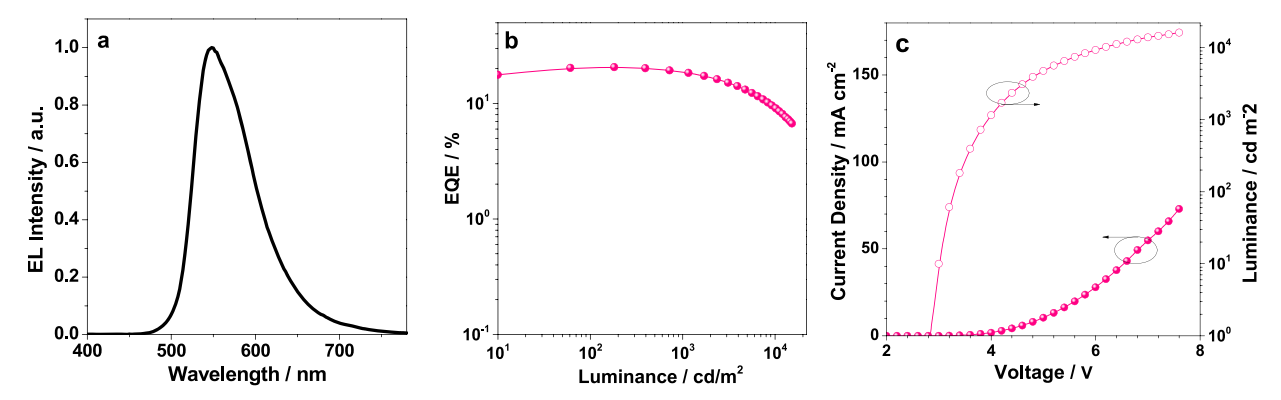


Figure 5. Electroluminescence device data: (a) EL spectrum; (b) EQE-L curve; (c) J-V-L curves. Device architecture: ITO/HATCN (5 nm)/TAPC (25 nm)/TCTA (5 nm)/CBP:10 wt % Ir2 (20 nm)/TmPyPB (55 nm)/LiF (1 nm)/Al.

respect to the other complexes, resulting in the strongest emission and longest lifetime among this series of complexes.

It is also worth noting that although the π -extended rigid benzo[h]quinoline C^N ligand lowered the emission energies of Ir1-Ir7, it prolonged the emission lifetimes for most of the complexes in all solvents (except for Ir1 and Ir6 in toluene, see Table S4 in the Supporting Information) by approximately 1 order of magnitude in comparison to that of the most relevant Ir(III) complex (0.69 μ s in MTHF) reported in the literature, which bears the 3-methyl-1-phenylbenzimidazol-3-ium NHC ligand and more flexible 2-phenylpyridine C^N ligands.²⁷ The prolonged lifetimes should be attributed to the drastically reduced k_{nr} values and/or k_r values in Ir1-Ir7. For example, the k_{nr} and k_r values for Ir3 (which has the same NHC ligand as that in complex 6 in ref 27) in THF are 4.17×10^5 and 1.18 \times 10⁵ s⁻¹, respectively, while these values for complex 6 in ref 27 in MTHF are 5.10×10^6 and 1.20×10^6 s⁻¹, respectively, assuming the same triplet quantum yield of 0.23 as that for Ir3. Apparently, replacing the more flexible 2-phenylpyridine ligand by the rigid benzo [h] quinoline ligand dramatically reduced the $k_{\rm nr}$ and $k_{\rm r}$ values for Ir3 in comparison to those of complex 6 in ref 27, resulting in a much longer lifetime (8.14 μ s for Ir3 in THF vs 0.69 μ s for complex 6 in ref 27 in MTHF) and slightly increased the emission quantum yield for Ir3 (0.22 in THF vs 0.19 for complex 6 in ref 27 in MTHF). An increased emission quantum yield and/or emission lifetime due to the incorporation of a rigid C^N or N^N ligand in Ir(III) complexes has been previously reported by our group for the monocationic $Ir(N^{\wedge}N)(C^{\wedge}N)_2^+$ -type complexes. Similar results are observed for the neutral Ir(NHC)(C^N)₂ type complexes reported in this work.

Transient Absorption (TA). To further explore the triplet excited-state characteristics of complexes Ir1-Ir7, a TA study was carried out in deaerated toluene solutions for all complexes. The TA spectra of Ir1-Ir7 immediately after 355 nm excitation are shown in Figure 4, and the time-resolved spectra are provided in Figure S9 in the Supporting Information. The TA band maxima, the triplet excited state lifetimes, and quantum yields are summarized in Table 2. The TA spectral features of all complexes resemble each other, all exhibiting a broad structureless positive absorption band in the region of 460-700 nm. However, the TA band maxima differ slightly, with electron-withdrawing substituents, especially the CN substituent, causing a noticeable blue shift, while electrondonating substituents showing a minor effect in comparison to that of Ir3. The major difference appeared at 380-450 nm, probably due to the different ground-state absorption in this

region. The triplet lifetimes deduced from the decay of TA signals matched well with the respective lifetimes obtained from the decay of emission signals, implying that the transient absorbing excited states are the emitting excited states: i.e., the C^N ligand-centered $^3\pi$, π^* state mixed with 3 MLCT configurations.

Phosphorescent OLEDs (PhOLEDs). Among this series of complexes, Ir2 possessed the highest emission quantum yields in all of the solvents studied. Thus, we chose this complex as the emitter for fabrication of a prototype electroluminescence (EL) device. The device architecture consisted of ITO/HATCN (5 nm)/TAPC (25 nm)/TCTA (5 nm)/CBP:10 wt % Ir2 (20 nm)/TmPyPB (55 nm)/LiF (1 nm)/Al. The data for the device performances, such as the luminance (L), current efficiency (η_c), power efficiency (η_p), and EQE, are summarized in Table 5. The obtained EL spectrum, EQE-L curve, and J-V-L curves are shown in Figure 5. The EL spectral feature and the emission band maximum (548 nm) resemble those of its photoluminescence in CH₂Cl₂, THF, and CH₃CN solutions (Figure S6 in the Supporting Information). Thus, the parentage of the EL is assigned to the triplet excited state of the dopant: namely, the 3 MLCT/ $^3\pi$, π^* state. The turn-on voltage (V_{on}) of this device was 2.9 V. In terms of the brightness, the maximum current efficiency (η_c) and external quantum efficiency (EQE) are 71.29 cd A^{-1} and 20.6%, respectively. Note that the device did not suffer from serious efficiency roll-off even at high brightness (Figure 5b). In comparison to the performance of a blue OLED using (2-(2,4-difluorophenyl)pyridine)₂Ir-(NHC) as the emitter,²² the OLED based on **Ir2** exhibited a lower turn-on voltage, doubled η_c and EQE, and almost 4-fold higher maximum luminance. These results demonstrate the potential of using these types of complexes as yellow emitters for OLED applications.

CONCLUSIONS

I

Seven neutral cyclometalated Ir(III) complexes bearing the benzo[h]quinoline C^N ligand and different 1-phenylbenzimidazole (NHC) ancillary ligands with substituents at the C4′ of the phenyl ring or C5 of the NHC ligand were synthesized and characterized. The influence of the electron-donating or -withdrawing substituents on their photophysical properties was investigated. All complexes exhibit ${}^1\pi$, π^* / 1 CT/ 1 d,d transitions at ca. 440 nm and yellow ${}^3\pi$, π^* / 3 MLCT emission at room temperature in fluid solutions. They all exhibited broad triplet transient absorption at 460–700 nm with similar

spectral features. Generally, electron-withdrawing substituents caused minor blue shifts of the low-energy absorption band and the emission band, while the electron-donating substituents induced red shifts somewhat. Although the effects of the substituents at the NHC ligand on the T₁ state energies of these complexes are quite minor, the effects on the T₁ lifetimes and emission quantum yields are drastic. The most emissive complex, Ir2, was utilized as the dopant for PhOLED fabrication. The obtained device displayed a yellow emission with a maximum current efficiency of 71.29 cd A⁻¹, a maximum luminance of 32747 cd m⁻², a maximum EQE of 20.6%, a low turn-on voltage (2.9 V), and a low efficiency rolloff. In comparison to the reported blue OLED using (2-(2,4difluorophenyl)pyridine)2Ir(NHC) as the emitter, the OLED based on Ir2 exhibited a lower turn-on voltage, doubled η_c and EQE, and almost 4-fold higher maximum luminance. These results demonstrate the potential of using these types of complexes as yellow emitters for OLED applications.

ASSOCIATED CONTENT

S Supporting Information

The Supporting Information is available free of charge on the ACS Publications website at DOI: 10.1021/acs.inorg-chem.9b01678.

Molecular structures of HATCN, TAPC, TCTA, CBP, and TmPyPB, crystallographic data of single crystal of Ir1, schematical view of the dihedral angle between the phenyl ring and the benzimidazole moiety in the crystal structure of Ir1, comparison of the experimental and calculated UV-vis absorption spectra of complexes Ir1-Ir7 in toluene, normalized UV-vis absorption and emission spectra of Ir1-Ir7 in different solvents, comparison of the emission spectra of Ir1-Ir7 and the calculated emission energies, the natural transition orbitals (NTOs) representing transitions contributing to the major absorption bands of Ir1-Ir7, the emission characteristics of Ir1-Ir7 in different solvents, comparison of the emission spectra of Ir2-Ir7 in MTHF at room temperature and 77 K, the time-resolved nanosecond transient absorption spectra of Ir1-Ir7 in toluene, and the full author list for ref 36 (PDF)

Accession Codes

CCDC 1923140 contains the supplementary crystallographic data for this paper. These data can be obtained free of charge via www.ccdc.cam.ac.uk/data_request/cif, or by emailing data_request@ccdc.cam.ac.uk, or by contacting The Cambridge Crystallographic Data Centre, 12 Union Road, Cambridge CB2 1EZ, UK; fax: +44 1223 336033.

AUTHOR INFORMATION

Corresponding Author

*W.S.: e-mail, Wenfang.Sun@ndsu.edu; tel, 701-231-6254; fax, 701-231-8831.

ORCID ®

Bingqing Liu: 0000-0002-1540-2235

Mohammed A. Jabed: 0000-0001-8552-0301 Erik K. Hobbie: 0000-0001-6158-8977 Svetlana Kilina: 0000-0003-1350-2790 Anjun Qin: 0000-0001-7158-1808 Wenfang Sun: 0000-0003-3608-611X

Notes

The authors declare no competing financial interest.

ACKNOWLEDGMENTS

W.S. and S.K. acknowledge the financial support from the National Science Foundation (DMR-1411086 and CHE-1800476) for complex synthesis, characterization, and computational simulation of the optical spectra. S.K. is grateful to the US Department of Energy (DE-SC008446) for financial support and the Center for Computationally Assisted Science and Technology (CCAST) at North Dakota State University and the National Energy Research Scientific Computing Center (NERSC) allocation Award No. 86678 (supported by the Office of Science of the Department of Energy under Contract No. DE-AC02-05CH11231) for computer access and administrative support.

REFERENCES

- (1) Jung, Y.; Lippard, S. J. Direct Cellular Responses to Platinum—Induced DNA Damage. *Chem. Rev.* **2007**, *107*, 1387–1407.
- (2) Dixon, I. M.; Collin, J.-P.; Sauvage, J.-P.; Flamigni, L.; Encinas, S.; Barigelletti, F. A Family of Luminescent Coordination Compounds: Iridium(III)Polyimine Complexes. *Chem. Soc. Rev.* **2000**, 29, 385–391.
- (3) Lee, S.; Kim, S.–O.; Shin, H.; Yun, H.–J.; Yang, K.; Kwon, S.–K.; Kim, J.–J.; Kim, Y.–H. Deep–Blue Phosphorescence from PerfluoroCarbonyl–Substituted Iridium Complexes. *J. Am. Chem. Soc.* **2013**, *135*, 14321–14328.
- (4) Tsuboyama, A.; Iwawaki, H.; Furugori, M.; Mukaide, T.; Kamatani, J.; Igawa, S.; Moriyama, T.; Miura, S.; Takiguchi, T.; Okada, S.; Hoshino, M.; Ueno, K. Homoleptic Cyclometalated Iridium Complexes with Highly Efficient Red Phosphorescence and Application to Organic Light—Emitting Diode. *J. Am. Chem. Soc.* 2003, 125, 12971—12979.
- (5) Zysman-Colman, E.; Slinker, J.-D.; Parker, J.-B.; Malliaras, G.-G.; Bernhard, S. Improved Turn-On Times of Light-Emitting Electro-chemical Cells. *Chem. Mater.* **2008**, *20*, 388–396.
- (6) Bolink, H.–J.; Cappelli, L.; Coronado, E.; Grätzel, M.; Orti, E.; Costa, R.–D.; Viruela, P.–M.; Nazeeruddin, M.–K. Stable Single–Layer Light–Emitting Electrochemical Cell Using 4,7–Diphenyl–1,10–phenan–throline–bis(2–phenylpyridine)iridium(III) Hexafluorophosphate. *J. Am. Chem. Soc.* **2006**, *128*, 14786–14787.
- (7) Mydlak, M.; Bizzarri, C.; Hartmann, D.; Sarfert, W.; Schmid, G.; De Cola, L. Positively Charged Iridium(III) Triazole Derivatives as Blue Emitters for Light–Emitting Electrochemical Cells. *Adv. Funct. Mater.* **2010**, *20*, 1812–1820.
- (8) Nam, J. S.; Kang, M.-G.; Kang, J.; Park, S.-Y.; Lee, S. J. C.; Kim, H.-T.; Seo, J. K.; Kwon, O.-H.; Lim, M. H.; Rhee, H.-W.; Kwon, T.-H. Endoplasmic Reticulum-Localized Iridium(III) Complexes as Efficient Photodynamic Therapy Agents via Protein Modifications. J. Am. Chem. Soc. 2016, 138, 10968–10977.
- (9) Liu, B.; Monro, S.; Lystrom, L.; Cameron, C. G.; Colón, K.; Yin, H.; Kilina, S.; McFarland, S. A.; Sun, W. Photophysical and Photobiological Properties of Dinuclear Iridium(III) Bis—tridentate Complexes. *Inorg. Chem.* **2018**, *57*, 9859—9872.
- (10) Maggioni, D.; Galli, M.; D'Alfonso, L.; Inverso, D.; Dozzi, M. V.; Sironi, L.; Iannacone, M.; Collini, M.; Ferruti, P.; Ranucci, E.; D'Alfonso, G. A. Luminescent Poly(amidoamine)—Iridium Complex as a New Singlet—Oxygen Sensitizer for Photodynamic Therapy. *Inorg. Chem.* **2015**, *54*, 544–553.
- (11) Li, Y.; Dandu, N.; Liu, R.; Hu, L.; Kilina, S.; Sun, W. Nonlinear Absorbing Cationic Iridium(III) Complexes Bearing Benzothiazolyl—fluorene Motif on the Bipyridine (N^N) Ligand: Synthesis, Photophysics and Reverse Saturable Absorption. *ACS Appl. Mater. Interfaces* **2013**, *5*, 6556–6570.
- (12) Li, Y.; Dandu, N.; Liu, R.; Li, Z.; Kilina, S.; Sun, W. Effects of Extended π -Conjugation in Phenanthroline (N^N) and Phenyl-

pyridine (C^N) Ligands on the Photophysics and Reverse Saturable Absorption of Cationic Heteroleptic Iridium(III) Complexes. *J. Phys. Chem. C* **2014**, *118*, 6372–6384.

- (13) Sun, W.; Pei, C.; Lu, T.; Cui, P.; Li, Z.; McCleese, C.; Fang, Y.; Kilina, S.; Song, Y.; Burda, C. Reverse Saturable Absorbing Cationic Iridium(III) Complexes Bearing the 2–(2–Quinolinyl)quinoxaline Ligand: Effects of Different Cyclometalating Ligands on Linear and Nonlinear Absorption. *J. Mater. Chem. C* **2016**, *4*, 5059–5072.
- (14) Wang, C.; Lystrom, L.; Yin, H.; Hetu, M.; Kilina, S.; McFarland, S. A.; Sun, W. Increasing the Triplet Lifetime and Extending the Ground–State Absorption of Biscyclometalated Ir(III) Complexes for Reverse Saturable Absorption and Photodynamic Therapy Applications. *Dalton Trans* **2016**, *45*, 16366–16378.
- (15) Wang, L.; Cui, P.; Kilina, S.; Sun, W. Towards Broadband Reverse Saturable Absorption: Investigating the Impact of Cyclometalating Ligand π -Conjugation on the Photophysics and Reverse Saturable Absorption of Cationic Heteroleptic Iridium Complexes. *J. Phys. Chem. C* **2017**, *121*, 5719–5730.
- (16) Li, Z.; Cui, P.; Wang, C.; Kilina, K.; Sun, W. Nonlinear Absorbing Cationic Bipyridyl Iridium(III) Complexes Bearing Cyclometalating Ligands with Different Degrees of π -Conjugation: Synthesis, Photophysics, and Reverse Saturable Absorption. *J. Phys. Chem. C* **2014**, *118*, 28764–28775.
- (17) Lo, K. K.-W.; Zhang, K. Y. Iridium(III) Complexes as Therapeutic and Bioimaging Reagents for Cellular Applications. *RSC Adv.* **2012**, *2*, 12069–12083.
- (18) You, Y. Phosphorescence Bioimaging Using Cyclometalated Ir(III) Complexes. Curr. Opin. Chem. Biol. 2013, 17, 699-707.
- (19) Li, Y.; Tan, C.-P.; Zhang, W.; He, L.; Ji, L.-N.; Mao, Z.-W. Phosphorescent Iridium(III)—Bis—N—Heterocyclic Carbene Complexes as Mitochondria—Targeted Theranostic and Photodynamic AnticancerAgents. *Biomaterials* **2015**, *39*, 95–104.
- (20) Sajoto, T.; Djurovich, P. I.; Tamayo, A.; Yousufuddin, M.; Bau, R.; Thompson, M. E.; Holmes, R. J.; Forrest, S. R. Blue and Near–UV Phosphorescence from Iridium Complexes with Cyclometalated Pyrazolyl or *N*–Heterocyclic Carbene Ligands. *Inorg. Chem.* **2005**, 44, 7992–8003.
- (21) Chang, C. F.; Cheng, Y. M.; Chi, Y.; Chiu, Y. C.; Lin, C. C.; Lee, G. H.; Chou, P. T.; Chen, C. C.; Chang, C. H.; Wu, C. C. Highly Efficient Blue–Emitting Iridium(III) Carbene Complexes and Phosphorescent OLEDs. *Angew. Chem., Int. Ed.* **2008**, *47*, 4542–4545.
- (22) Li, T. Y.; Liang, X.; Zhou, L.; Wu, C.; Zhang, S.; Liu, X.; Zuo, J. L. *N*-Heterocyclic Carbenes: Versatile Second Cyclometalated Ligands for Neutral Iridium(III) Heteroleptic Complexes. *Inorg. Chem.* **2015**, *54*, 161–173.
- (23) Wiegmann, B.; Jones, P. G.; Wagenblast, G.; Lennartz, C.; Münster, I.; Metz, S.; Kowalsky, W.; Johannes, H. H. A New Framework of a Heteroleptic Iridium(III)-Carbene Complex as a Triplet Emitting Material. *Organometallics* **2012**, *31*, 5223–5226.
- (24) Darmawan, N.; Yang, C.-H.; Mauro, M.; Raynal, M.; Heun, S.; Pan, J.; Buchholz, H.; Braunstein, P.; De Cola, L. Efficient Near-UV Emitters Based on Cationic Bis-Pincer Iridium(III) Carbene Complexes. *Inorg. Chem.* **2013**, *52*, 10756–10765.
- (25) Monti, F.; La Placa, M. G. I.; Armaroli, N.; Scopelliti, R.; Grätzel, M.; Nazeeruddin, M. K.; Kessler, F. Cationic Iridium(III) Complexes with Two Carbene-Based Cyclometalating Ligands: Cis Versus Trans Isomers. *Inorg. Chem.* **2015**, *54*, 3031–3042.
- (26) Chien, C.-H.; Fujita, S.; Yamoto, S.; Hara, T.; Yamagata, T.; Watanabe, M.; Mashima, K. Stepwise and One-pot Syntheses of Ir(III) Complexes with Imidazolium-Based Carbene Ligands. *Dalton Trans* **2008**, 916–923.
- (27) Tennyson, A. G.; Rosen, E. L.; Collins, M. S.; Lynch, V. M.; Bielawski, C. W. Bimetallic *N*-Heterocyclic Carbene-Iridium Complexes: Investigating Metal-Metal and Metal-Ligand Communication via Electrochemistry and Phosphorescence Spectroscopy. *Inorg. Chem.* **2009**, *48*, 6924–6933.
- (28) Nemcsok, D.; Wichmann, K.; Frenking, G. The Significance of π Interactions in Group 11 Complexes with N–Heterocyclic Carbenes. *Organometallics* **2004**, 23, 3640–3646.

(29) Fleetham, T.; Li, G.; Li, J. Phosphorescent Pt(II) and Pd(II) Complexes for Efficient, High-Color-Quality, and Stable OLEDs. *Adv. Mater.* **2017**, 29, 1601861.

- (30) Yang, H.; Miao, Z.; Chen, R. A Versatile and Efficient Cu-Catalyzed N-Arylation of Aromatic Cyclic Secondary Amines with Aryl Halides. *Lett. Org. Chem.* **2011**, *8*, 325–331.
- (31) Zhu, L.; Li, G.; Luo, L.; Guo, P.; Lan, J.; You, J. Highly Functional Group Tolerance in Copper—Catalyzed *N* Arylation of Nitrogen—Containing Heterocycles under Mild Conditions. *J. Org. Chem.* **2009**, *74*, 2200—2202.
- (32) Li, Z.; Cui, P.; Wang, C.; Kilina, S.; Sun, W. Nonlinear Absorbing Cationic Bipyridyl Iridium(III) Complexes Bearing Cyclometalating Ligands with Different Degrees of π -Conjugation: Synthesis, Photophysics, and Reverse Saturable Absorption. *J. Phys. Chem. C* **2014**, *118*, 28764–28775.
- (33) Carmichael, I.; Hug, G. L. Triplet triplet Absorption Spectra of Organic Molecules in Condensed Phases. *J. Phys. Chem. Ref. Data* **1986**, *15*, 1–250.
- (34) Kumar, C. V.; Qin, L.; Das, P. K. Aromatic Thioketone Triplets and Their Quenching Behaviour towards Oxygen and Di-t-butylnitroxy Radical. A Laser-Flash-Photolysis Study. *J. Chem. Soc., Faraday Trans.* 2 **1984**, *80*, 783–793.
- (35) Firey, P. A.; Ford, W. E.; Sounik, J. R.; Kenney, M. E.; Rodgers, M. A. J. Silicon Naphthalocyanine Triplet State and Oxygen. A Reversible Energy—transfer Reaction. *J. Am. Chem. Soc.* **1988**, *110*, 7626—7630.
- (36) Frisch, M. J.; Trucks, G. W.; Schlegel, H. B.; Scuseria, G. E.; Robb, M. A.; Cheeseman, J. R.; Scalmani, G.; Barone, V.; Petersson, G. A.; Nakatsuji, H., et al. *Gaussian 16, Rev. B.01*; Gaussian, Inc.: Wallingford, CT, 2016.
- (37) Kohn, W.; Sham, L. J. Self-Consistent Equations Including Exchange and Correlation Effects. *Phys. Rev.* **1965**, *140*, A1133–A1138.
- (38) Yanai, T.; Tew, D. P.; Handy, N. C. A New Hybrid Exchange—Correlation Functional Using the Coulomb-Attenuating Method (CAM-B3LYP). *Chem. Phys. Lett.* **2004**, 393, 51–57.
- (39) Hay, P. J.; Wadt, W. R. Ab Initio Effective Core Potentials for Molecular Calculations. Potentials for K to Au Including the Outermost Core Orbitals. *J. Chem. Phys.* **1985**, 82, 299–310.
- (40) Clark, T.; Chandrasekhar, J.; Spitznagel, G. W.; Schleyer, P. V. R. Efficient Diffuse Function-Augmented Basis Sets for Anion Calculations. III. The 3-21+G Basis Set for First-Row Elements, Li–F. J. Comput. Chem. 1983, 4, 294–301.
- (41) Barone, V.; Cossi, M.; Tomasi, J. Geometry Optimization of Molecular Structures in Solution by the Polarizable Continuum Model. *J. Comput. Chem.* **1998**, *19*, 404–417.
- (42) Casida, M. E.; Jamorski, C.; Casida, K. C.; Salahub, D. R. Molecular Excitation Energies to High-Lying Bound States from Time-Dependent Density-Functional Response Theory: Characterization and Correction of the Time-Dependent Local Density Approximation Ionization Threshold. *J. Chem. Phys.* **1998**, *108*, 4439–4449.
- (43) Adamo, C.; Barone, V. Toward Reliable Density Functional Methods without Adjustable Parameters: The PBE0Model. *J. Chem. Phys.* **1999**, *110*, 6158–6170.
- (44) Liu, B.; Lystrom, L.; Kilina, S.; Sun, W. Effects of Varying the Benzannulation Site and -Conjugation of the Cyclometalating Ligand on the Photophysics and Reverse Saturable Absorption of Monocationic Iridium(III) Complexes. *Inorg. Chem.* **2019**, *58*, 476–488.
- (45) Cai, Z.-L.; Crossley, M. J.; Reimers, J. R.; Kobayashi, R.; Amos, R. D. Density Functional Theory for Charge Transfer: The Nature of the N-Bands of Porphyrins and Chlorophylls Revealed through CAM-B3LYP, CASPT2, and SAC-CI Calculations. *J. Phys. Chem. B* **2006**, *110*, 15624–15632.
- (46) Komjáti, B.; Urai, Á.; Hosztafi, S.; Kökösi, J.; Kováts, B.; Nagy, J.; Horváth, P. Systematic Study on the TD-DFT Calculated Electronic Circular Dichroism Spectra of Chiral Aromatic Nitro

Compounds: A Comparison of B3LYP and CAM-B3LYP. Spectrochim. Acta, Part A 2016, 155, 95-102.

- (47) Ziegler, T.; Rauk, A.; Baerends, E. J. On the Calculation of Multiplet Energies by the Hartree-Fock-Slater Method. *Theoret. Chim. Acta* 1977, 43, 261–271.
- (48) Baruah, T.; Olguin, M.; Zope, R. R. Charge Transfer Excited State Energies by Perturbative Delta Self Consistent Field Method. *J. Chem. Phys.* **2012**, *137*, 084316.
- (49) Badaeva, E.; Albert, V. V.; Kilina, S.; Koposov, A.; Sykora, M.; Tretiak, S. Effect of Deprotonation on Absorption and Emission Spectra of Ru(II)-bpy Complexes Functionalized with Carboxyl Groups. *Phys. Chem. Chem. Phys.* **2010**, *12*, 8902–8913.
- (50) Martin, R. L. Natural Transition Orbitals. J. Chem. Phys. 2003, 118, 4775.
- (51) Humphrey, W.; Dalke, A.; Schulten, K. VMD: Visual Molecular Dynamics. *J. Mol. Graphics* **1996**, *14*, 33–38.
- (52) Sheldrick, G. M. Crystal structure refinement with SHELXL. Acta Crystallogr., Sect. C: Struct. Chem. 2015, C71, 3–8.
- (53) Dolomanov, O. V.; Bourhis, L. J.; Gildea, R. J.; Howard, J. A. K.; Puschmann, H. OLEX2: a complete structure solution, refinement and analysis program. *J. Appl. Crystallogr.* **2009**, *42*, 339–341.
- (54) Farrugia, L. J. WinGX and ORTEP for Windows: An Update. J. Appl. Crystallogr. 2012, 45, 849–854.
- (55) Liu, B.; Lystrom, L.; Kilina, S.; Sun, W. Effects of Varying the Benzannulation Site and π Conjugation of the Cyclometalating Ligand on the Photophysics and Reverse Saturable Absorption of Monocationic Iridium(III) Complexes. *Inorg. Chem.* **2019**, *58*, 476–488.
- (56) Liu, B.; Lystrom, L.; Brown, S. L.; Hobbie, E. K.; Kilina, S.; Sun, W. Impact of Benzannulation Site at the Diimine (N[^]N) Ligand on the Excited-State Properties and Reverse Saturable Absorption of Biscyclometalated Iridium(III) Complexes. *Inorg. Chem.* **2019**, *58*, 5483–5493.
- (57) Pei, C.; Cui, P.; McCleese, C.; Kilina, S.; Burda, C.; Sun, W. Heteroleptic Cationic Iridium(III) Complexes Bearing Naphthalimidyl Substituents: Synthesis, Photophysics and Reverse Saturable Absorption. *Dalton Trans* **2015**, *44*, 2176–2190.